Phase transitions, coexistence and crystal growth dynamics in ionic nanoclusters: Theory and simulation

Pedro C.R. Rodrigues *, Fernando M.S. Silva Fernandes

Centre of Molecular Sciences and Materials, Molecular Simulation Group, Department of Chemistry and Biochemistry, Faculty of Sciences, University of Lisboa Campo Grande, Bloco C8, 1749-016 Lisboa, Portugal

ARTICLE INFO

ABSTRACT

A review of our work on phase transitions, coexistence and crystal growth dynamics in ionic nanoclusters is presented. The foundations and limitations of the proposed models are discussed and perspectives for extended treatments are given. Additionally, supported on a compilation of the asymptotic behaviour of the properties towards bulk conditions, new results concerned with the operational meaning of the thermodynamic limit are also presented. Some topics are complemented with link references to on-line animations that provide a visualisation of the focused behaviours. The simulations were carried out by molecular dynamics on KCl, NaCl, LiCl and NaI clusters.

© 2010 Elsevier B.V. All rights reserved.

1. Introduction

A substance can freeze at a temperature different from its melting point. This phenomenon, called hysteresis, is usually associated with metastable conditions at high cooling rates of a melted liquid and reversible paths are expected from carefully managed experiments. Yet, even simple and pure substances can show irreversible melting, that is, cooling the melt never, or seldom, results in a crystal even slowing down the cooling rate or seeding the melt [1]. In such cases, a phase change is not completely characterised by the melting point, for example, and more complex paths can arise. Consequently, a particular care should be taken in order to choose convenient properties that unambiguously characterise a system during a phase change. In this context, regardless of its constitution, a system with a finite size (cluster) generally presents additional features that can not be ignored, due to the energy contributions of the interfaces. The outside interfacial contributions, in particular, prevent the system to remain at constant temperature during a phase conversion [2–10], often resulting in a strong non-linear behaviour.

The concept of aggregate, or cluster, is presented in the literature in several contexts and interpretations such as regions with differentiated structure [11], an isolated entity surrounded by vacuum [12], or even an abstract entity defined by a set of particles confined in a short space scale [13]. All these definitions, however, have in common the restriction of a small number of particles relatively to the bulk systems. Several workers have performed simulations in unconstrained clusters with tens to thousands of particles by computing properties like temperature, configurational and total energies, diffusion coefficients, autocorrelation functions [2–10] and Liapunov exponents [14]. The studied clusters include noble gases [2,3,6–8], mixed system [15], alkali halides [9,16–22], water [23] and metals [24], by using effective potentials. Also, for example, TeF6 [25,26], pure [27,28] and doped [29] sodium, and LiCl [30] by using *ab initio* methods. Some studies include the application of external fields [31] and others are performed in supercritical fluids [32].

The main objective of the present paper is to review the strategies and models proposed to deal with cluster behaviours during phase changes, coexistence and crystal growth, discuss their foundations and limitations and to trace out some possible developments. Additionally, the collected simulation results and the developed models are used to estimate cluster sizes needed to fulfil the thermodynamic limit conditions.

Computational remarks are presented in Section 2. A few examples of properties computed during phase transitions and coexistence of clusters, many of them relevant to the construction of a phase coexistence model, are presented in Section 3. Section 4 is devoted to the introduction of the phase coexistence model. In Section 5 several model application examples are given. A discussion on the meaning of the thermodynamic limit, supported on the previous results and models, is made in Section 6. Finally, some perspectives of future developments are given in Section 7.

* Corresponding author. Tel.: +351 21750000x26140.
  E-mail addresses: reis@fc.ul.pt (P.C.R. Rodrigues), fmfernandes@fc.ul.pt (F.M.S.S. Fernandes).

2. Computational remarks

Full details of the computations are given elsewhere [9,16,17,19–22]. Here, only a few details are recalled.

A key strategy to unravel phase coexistence, used in most of the calculations, is heating or cooling the clusters under controlled energy fluxes, that is, rescaling the velocities by a factor (slightly greater or less than 1, respectively), subsequently isolating the systems, calculating their properties after a complete relaxation, and then imposing the next rescaling. This process (designated as "constant energy or fixed energy process" in what follows) allows the systems to adjust the internal kinetic and potential energies, keeping the total energy constant. Therefore, generally, melting decreases and freezing increases the temperature of the clusters.

Most of the molecular dynamics computations have been performed using the Born–Mayer–Huggins (BMH) potential:

$$\phi_{ij}(r) = \frac{z_i z_j e^2}{r} + c_{ij} b \exp\left[\frac{\sigma_{ij} - r}{d}\right] - \frac{C_{ij}}{r^6} - \frac{D_{ij}}{r^8} \quad (1)$$

with the parameters given by Watts and McGee [33]. Additionally, in order to analyse the relative stability of the clusters at 0 K we have also done some calculations with the Michielsen–Woerlee–Graaf (MWG) potential:

$$\phi_{ij}(r) = \frac{z_i z_j e^2}{r} + \frac{b}{r^l} \exp\left[k_{ij}(\sigma_{ij}^m - r^m)\right] - \frac{C_{ij}}{r^6} - \frac{D_{ij}}{r^8} \quad (2)$$

with the parameters given by Michielsen et al. [34] for $l = 4$ and $m = 1$. It is well-known that these interaction models, despite being rigid-ion and effective potentials, reproduce some bulk properties of alkali halides and other substances fairly well. Recently, we have reported [35] an extensive study, by molecular dynamics and free energy calculations, of the phase diagrams for bulk KCl and NaCl, also using those models. A generalised and accurate reproduction of experimental results requires more sophisticated models. It is noteworthy, however, that potential details and accuracy have little, if any, influence in the structure of the theoretical models presented ahead.

Verlet's leapfrog algorithm [36] for the numerical integration of Newton's equations of motion, with a time step of 5×10^{-15} s, has been used in all simulations. Equilibration runs up to 10^3 steps have been used for thermal relaxation, insuring that the production starting temperatures remain inside average fluctuation intervals. Thermal properties have been calculated with production runs of 5×10^3 to 5×10^5 steps for each point, depending on the size of the clusters and the phase transition region. A set of 300–600 points has been computed for each plot. The determination of the velocity auto-correlation functions, which are essential to assess many properties along the phases coexistence, has been based on runs of $1.6 \times 10^4 - 4 \times 10^6$ time steps with a time origin at every fifth step.

3. Phase change examples

The following Sections 3.1 and 3.2 contain some results obtained for phase changes, coexistence and nucleation in clusters. These results, in particular the ones concerning nucleation, give important information for the construction of the phase coexistence model. They will also help to identify the roots of the model limitations and to trace out possible extensions.

3.1. Melting

The black curves in Fig. 1 show the melting behaviour for KCl clusters of different sizes by slow heating the solid. All the clusters present first-order phase transitions for which the estimated limit
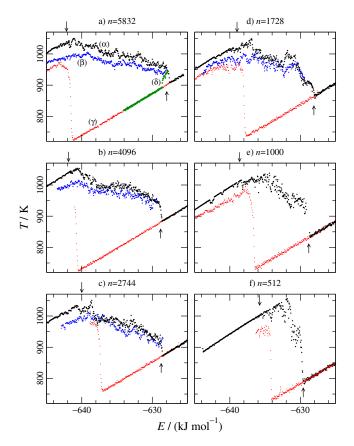

Fig. 1. Phase change diagrams of KCl clusters. Heating is in black (α), nucleated cooling is in blue (β), non-nucleated cooling is in red (γ), cooling with ineffective residual crystallite is in green (δ). Melting onset ($\downarrow$), melting end ($\uparrow$). (For interpretation of the references to color in this figure legend, the reader is referred to the web version of this paper.)

points for prevalence of the solid are given in Table 1 (see also the arrows in the figure). As expected, the melting temperatures approach the experimental bulk value as the size of the clusters increases. For clusters whose sizes are greater than 512 ions the melting proceeds with the presence of phase coexistence in a single aggregate, approaching a phase change at constant temperature as the size increases. At the end of melting there is a complete breakdown of the crystal and the curves follow the usual liquid-like behaviour.

Fig. 2, displays snapshots of the 4096 ions cluster at the onset and the final stage of the melting showing evidence of sustained solid–liquid coexistence. It should be noticed that for cluster sizes over ~1000 ions the solid and liquid phases are simultaneously present and dynamically sustained in a single cluster. By slowly transferring energy to or from the system there is a reversible move along the solid–liquid coexistence. This indicates that the

Table 1
Melting points (T_m/K) and total energies ($E_{tot}/kJ\ mol^{-1}$) for KCl clusters. Experimental bulk values are included for comparison.

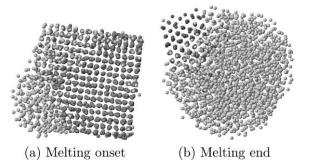| n	T_m	E_{tot}
512	~1000	~ − 636
1000	1008	−638.66
1728	1040	−639.12
2744	1046	−640.13
4096	1037	−641.84
5832	1049	−642.27
Exp. [37]	1045	–
Exp. [38]	1044	–

Fig. 2. Phase coexistence during the melting of the 4096 KCl cluster.

cluster is equilibrated. Moreover, dynamical alternation between melted corners of the cluster lattices is observed as much as the simulations evolve in time. It is interesting to note that the snapshots confirm the well-known fact that alkali halides are nonself-wetting materials [43].

Using a method based on the velocity auto-correlation functions of the ions, reported elsewhere [16], it is possible to estimate the molar fraction of the liquid in the coexistence regions as a function of energy (an example is given in Section 5.2). Despite the molar fractions oscillate there are no dynamical "jumps" between solid and liquid forms.

Table 2 contains the enthalpies of melting and Table 3 presents the heat capacities before and after melting calculated from the temperature–energy curves. These results also approach the experimental bulk values and the heat capacities increase from the solid to the liquid phases.

Different systems may present rather different behaviours during phase coexistence, as can be seen ahead in Section 5 where model application examples to NaCl and NaI are presented. A special example, among the studied cases, is the two solid phases detected in LiCl clusters. The temperature as a function of total energy, for different LiCl cluster sizes, is represented in Fig. 3, where the starting states for the heating curves have been cubic structures (cut from a perfect rock salt crystal). The heating curves starting from hexagonal structures and other details are reported elsewhere [20]. The coexistence regions show well distinguishable "plateaus" connected by abrupt slopes. In order to confirm that, for a given cluster size, these features correspond to different solid phases, snapshots have been collected from each "plateau" in the neighbourhood of the slopes that connect them. Fig. 4 displays snapshots for the 1728 ions cluster in convenient perspectives. In addition to the symmetry change, there are some other noticeable differences, such as: the liquid phase wets more extensively the hexagonal phase than the cubic one; the cubic structure appears in a distorted form that is wider near the liquid phase; the profile of the liquid wetting the cubic phase is similar to the one over a pair of contiguous faces in the hexagonal structure.

Fig. 3 also shows some regular behaviours: (i) during heating, lithium chloride presents a double phase transition, cubic →

Table 3
Heat capacities (C_p/JK^{-1} mol^{-1}) for solid and liquid KCl clusters of different sizes at 940 K and 1045 K. Experimental bulk values are included for comparison.

n	Solid		Liquid	
	940 K	1045 K	940 K	1045 K
512	67.9	–	72.3	69.2
1000	68.2	–	69.6	64.7
1728	66.5	–	72.7	71.6
2744	66.4	–	71.3	68.4
4096	65.6	71.9	72.4	70.7
5832	63.6	66.2	72.0	70.0
10648			71.6	69.1
From [42]	–	64.9		
Exp. [42]	–	66.9		
Exp. [39,38]	64.4	69.3		73.6

cubic + liquid → hexagonal + liquid; (ii) spontaneous nucleation (see Ref. [17]) of the supercooled liquid droplet occurs, always, with the formation of a cubic structure; and (iii) for the lower cooling rates, as in the 1000 ions cluster, a double transition, liquid → cubic + liquid → hexagonal + liquid, at fixed energy, is observed. The last feature is consistent with the nucleation of the hexagonal phase in the liquid over the cubic phase, since no direct spontaneous liquid → hexagonal + liquid transition is observed. Thus, the cubic + liquid → hexagonal + liquid transition mechanism seems to have an intermediate step where the two solid phases coexist with the liquid. Then, due to the growth of the hexagonal phase, the temperature shall increase until the cubic phase is completely melted. However, since this is a relatively fast process, further refined calculations are needed to clarify such details. The presence of the two solid phases can also be observed in the liquid molar fractions obtained by means of the method based on the velocity autocorrelation functions already referred to. This presence is expressed as two well-distinguishable non-co-linear and nearly parallel curves [17]. The transition from one to another occurs precisely at the same energy as the respective slope in Fig. 3.

3.2. Freezing

Figs. 1 and 3, also display the freezing curves obtained from KCl and LiCl totally melted configurations, and from configurations not completely melted containing residual crystallites, by slowly cooling the systems. The freezing process from supercooled liquid KCl configurations plus a solid seed (heterogeneous nucleation) is displayed ahead in separate diagrams.

3.2.1. Spontaneous nucleation

The diagrams of Fig. 1 indicate that hysteresis cycles show up when the freezing process is carried out from totally melted configurations since spontaneous crystallisation occurs at lower temperatures/energies than the ones corresponding to the complete crystal breakdown in the melting (see black and red curves). The temperature at which spontaneous crystallisation occurs is, approximately, the same ($\sim$730 K) for cluster sizes over 512. It may be suggested that this temperature (T_{sc}) corresponds to the supercooling limit of the liquid clusters according to the following analysis.

Assuming homogeneous nucleation, at least one critical nucleus must be formed in a liquid droplet of volume V so that crystallisation occurs. Then, the attainable limit of supercooling for the liquid droplet, that is, the homogeneous nucleation reduced temperature $\theta_{sc} = T_{sc}/T_m$, is [11]:

$$1 = \frac{VT_m}{dT/dt} \int_{1}^{\theta_{sc}} J(\theta) d\theta \qquad (3)$$

Table 2
Enthalpies of melting for KCl clusters of different sizes (Δh/kJ mol^{-1}).

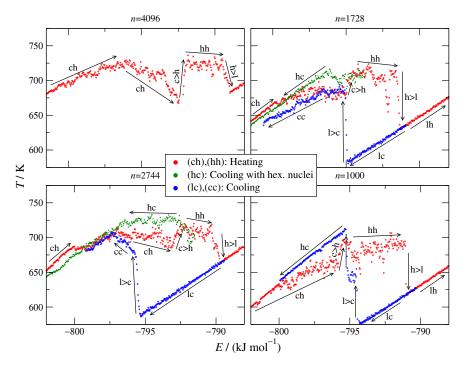| n	Δh
512	22.73
1000	23.13
1728	24.06
2744	24.24
4096	24.81
5832	25.04
Exp. [39,38]	26.4
Exp. [40]	25.5
Exp. [41]	26.5

Fig. 3. Temperature as a function of total energy for LiCl clusters of 1000, 1728, 2744 and 4096 ions, showing the occurrence of more than one solid phase. (ch) cubic heating; (cc) cubic cooling; (hh) hexagonal heating; (hc) cooling with residual hexagonal nuclei; (lc) liquid cooling; ($c > h$) cubic to hexagonal; ($h > l$) hexagonal to liquid; ($l > c$) liquid to cubic. Arrows indicate the directions of the heating and cooling paths.
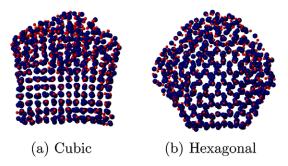

(a) Cubic   (b) Hexagonal

Fig. 4. Cubic and hexagonal symmetries in the 1728 ions cluster of LiCl during the melting starting from a cubic solid.

Fig. 5. θ_{sc} as a function of $nT_m/(dT/dt)$ for a set of KCl clusters. The dashed curve is a guide for the eye.

where T_m is the bulk melting temperature, dT/dt is the cooling rate and J is the rate of homogeneous nucleation, that is, the number of critical nuclei per unit volume and unit time. Fig. 5 shows θ_{sc} as a function of $nT_m/(dT/dt)$ computed from the previous data and from additional computations [17]. The overall profile of the curve is, within the margin of statistical errors, in close agreement with the predictions of the classical nucleation theory, except (also detectable in Fig. 1 and Table 4) in the 2744 ions cluster which represents a fortuitous event of premature nucleation. The experimental attainable limit of supercooling for KCl is 0.836 (874 K) [11] while the average value of the plateau in Fig. 5 is 0.697 (731 K). This is consistent with the fact that the sizes of our clusters are of the order of 1 nm (compared to typical droplet sizes of 1 μm in cloud chambers and 10 μm in emulsions) and the cooling rates in the simulations are considerably higher than the experimental ones. A larger amount of data with improved statistics is being produced to allow the computation of the rate of homogeneous nucleation as a function of θ and cluster size. This will presumably shed light on the time scale that one can expect for the formation of critical nuclei, as a function of both temperature and cluster size.
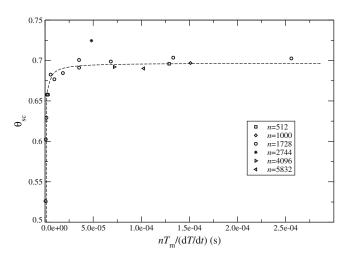
Table 4
Self diffusion coefficients, SDC, for KCl clusters of different sizes just before spontaneous crystallisation. Energies in kJ mol^{-1}, temperatures in K and self diffusion coefficients in 10^5 cm^2 s^{-1}.

n	Energy	T	SDC
1728	−637.68	734	2.90
2744	−636.86	760	3.26
4096	−640.33	726	2.73
5832	−640.82	728	2.74
10648	−641.27	735	2.71

Although vitrification is possible to occur in simulated clusters or bulk KCl, by applying instantaneous or very high cooling rates [44,9], it appears that the present simulations have prevented it.

In fact, it has been detected that such systems present a glass transition at $\theta \sim 0.3$ ($\sim$300 K). The temperatures in the present simulation are above this value. From Fig. 5 it can also be inferred that the probed conditions (cooling ratios and cluster sizes) are above (though not too far) the region where vitrification is concurrent with crystallisation. Moreover, the self-diffusion coefficients in the supercooled region show a liquid behaviour and have higher values than the ones of coexistent states [17].

Representing, for clarity, the solid molar fractions as a function of temperature (see Fig. 6), it is clear that the supercooled liquid, obtained from totally melted states, contains traces of solid-like ions. However, they do not form a single solid (pre-critical) nucleus inside the liquid droplet. On the contrary, they constitute sparse clouds of individual ions trapped by their neighbours (with lifetimes $\gtrsim 40$ ps) whose percentage increases as the temperature decreases. Table 5 contains the fitting coefficients to:

$$\frac{n_s}{n} = C \exp\left[\gamma(T - T_0)\right] \tag{4}$$

where n_s and n are the number of solid-behaved ions and the total number of ions, respectively. The curves have a steep increase at $\sim$730 K. The fitting coefficients seem to be uncorrelated with the size of the clusters and for the bigger ones the curves almost coincide. Considering that the probability of spontaneous nucleation increases with the fraction of solid-like ions in the supercooled liquid, the exponential form seems to describe the homogeneous nucleation process in the present clusters. These results help to understand the computational difficulty in obtaining the upper temperature points in Fig. 5 and strongly suggest the use of seeding to probe nucleation at higher temperatures.

3.2.2. Heterogeneous nucleation

As for the freezing process starting at configurations not completely melted containing residual crystallites, the behaviour is clearly different (see blue curves in Fig. 1) since the liquid already contains nuclei which mimic the seeds in heterogeneous nucleation. The hysteresis practically disappears and the freezing curves approach the melting ones. However, if the liquid is not sufficiently nucleated, then supercooling and hysteresis show up again (see green curve in Fig. 1).

The last observations called for a further analysis of heterogeneous nucleation by means of introducing external seeds as small crystallites that collide with the liquid droplet. In this way one can assess the critical nucleus sizes for an effective nucleation. We have firstly chosen a set of configurations at different energies of
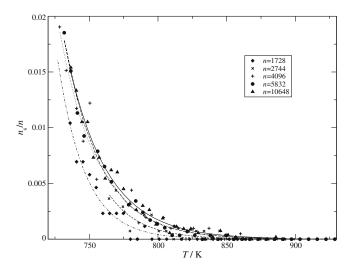
Table 5
Values of the exponent factor γ (in K^{-1}), and pre-factor C obtained, for KCl, from the fittings to Eq. (4).

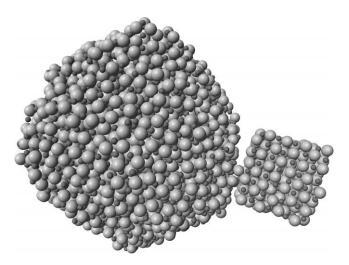| n	γ	C
1728	−0.038	0.011
2744	−0.026	0.008
4096	−0.031	0.017
5832	−0.038	0.022
10648	−0.033	0.020

Fig. 7. Snapshot of a KCl liquid droplet (n = 5832–512) in the presence of a small crystal seed (n = 512).

the 5832-ion cluster, in the supercooled liquid branch, and extracted 512 ions from them. After the thermal stabilisation of the resulting liquid droplets we have added one seed (a solid crystallite with 512 ions) in the neighbourhood of the droplets (see Fig. 7) and then followed the time evolution of the seeded droplets displayed in Fig. 8. The general evolution shows that the temperature increases rapidly with time when the energy is relatively low, until it reaches the solid or the coexistence solid–liquid curves. From there on the temperature stabilises along the time.[1] The rate of temperature variation decreases as the energy increases and from a value of energy $\sim$−630 kJ mol^{-1} upwards the temperature ceases to increase and the system reaches the same supercooled states obtained by cooling the non-nucleated liquid droplet.

We have also performed simulations starting with the same supercooled liquid droplet of 5832 ions and using smaller seeds with 64 and 216 ions. In these cases the liquid droplets have approximately the same size as for the 512-ion seed (5832–64 and 5832–216 ions, respectively). In the case of the 64 ions crystallite, the seed is ineffective in all the existence range of the probed supercooled liquid, even for values of energy/temperature near the occurrence of spontaneous nucleation ($\sim$730 K). As for the case of the 216 ions crystallite, the seed is effective, but only in a shorter range of temperature/energy than in the case of the 512 ions seed. Above 785 K the seed looses its efficiency. However, below that temperature the behaviour of the system, namely its time evolution periods, is similar to the 512 case. Thus, it seems that the difference between the results obtained with seeds of different sizes is only in the temperature below which the seed is effective.

The previous quantitative results and analysis are complemented by some instantaneous views of the studied systems. In

Fig. 6. Fraction of solid-like ions, in the supercooled liquid, as a function of temperature for KCl clusters of different sizes(n).

---

[1] The noticeable gap near the middle of the energy axes is due to the shorter runs performed at these state points.
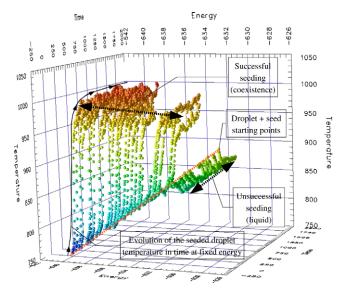
Fig. 8. Induced crystal growth dynamics (temperature evolution in time at fixed energy) of a supercooled KCl droplet ($n = 5832$–512) ions, using a seed of 512 ions. Bullets are coloured according to the system temperatures ranging from blue (for the lowest ones) to red (for the highest ones). Time in ps, temperature in K and total energy in kJ mol^{-1}. (For interpretation of the references to color in this figure legend, the reader is referred to the web version of this paper.)

fact, the perception of the phenomena can be enriched by dynamic perspectives following their evolution in time. To this end, we have produced some animation examples, available on-line, for the melting process [45], and for successful [46] and unsuccessful seeding [47] cases.

3.2.3. Sizes of critical nuclei

Accordingly to the classical nucleation theory [11,48], if a crystallite produced by a fluctuation in an infinite unstable liquid system is smaller than a critical size it shall shrink and disappear. If it is greater than the critical size the crystallite will grow until all the system becomes solid. This is due to the balance between two contributions to the free energy (the minimum reversible work of formation) that have opposite signs [11,48]. The free energy (work function) [11] to create an embryo inside a bulk liquid phase at a fixed temperature, T, and pressure, p, is:

$$W_{min}(T,p) = \sigma(T,p)F + n_e\Delta\mu(T,p) \tag{5}$$

where n_e is the number of particles in the embryo, F is the surface area of the embryo, $\sigma(T,p)$ is the interfacial solid–liquid surface tension and $\Delta\mu(T,p)$ is the difference between the chemical potentials of the stable and unstable phases. F depends on the embryo geometry and, in most cases, it is proportional to $n_e^{2/3}$. Because of the positive sign of the first term and the negative one of the second, together with the respective dependencies on n_e, Eq. (5) has a maximum at some value $n_e = n^*$, the so-called critical nucleus size. Embryos containing less than n^* particles shrink spontaneously, while embryos greater than n^* grow spontaneously. As such, for the formation of the new phase, the system must first overcome a free energy barrier by creating a critical nucleus, that is, the minimum size of the seed that is effective at a given temperature T. For cubic seeds, the average number of particles by one edge of the cube, n_a^*, can be derived from Eq. (5) [11,48,18]:

$$n_a^* = \frac{4\upsilon^{\frac{2}{3}}\sigma T_m}{(T_m - T)\Delta h} \tag{6}$$

where υ is the specific volume of the solid, T_m is the bulk melting temperature and Δh is the enthalpy of melting. Assuming that σ

and υ are independent on the temperature [11], Eq. (6) can be rewritten in the form:

$$\frac{n_a^*(T_m - T)}{T_m} = k \tag{7}$$

In the case of the 512 ions seed, $n_a^* = 8$, $T_m = 1049$ K and $T = 855$ K. Therefore, the value of k is 1.48 and the highest temperature at which other seeds are effective should be given by:

$$T = T_m - k\frac{T_m}{n_a^*} \tag{8}$$

For the 216 ions seed the predicted temperature is 790 K in good agreement with the simulation value of 785 K. In the case of the 64 ions seed the predicted temperature is 661 K well below the temperature of spontaneous crystallisation, and in accordance with the systematic destruction of the seed observed along the probed supercooled region.

We should point out that, apart from the assumption of σ and υ being independent on the temperature, the application of Eq. (6) to the present cases does not strictly obey to the conditions of its derivation. Indeed, the equation is obtained supposing homogeneous nucleation where the spontaneous critical nucleus is well inside the liquid, that is, completely wetted. It is well-known, however, that alkali halides are nonself-wetting materials as we have referred to before. Consequently, the seeds remain outside the liquid droplet during the crucial steps of the crystal growth process with their faces not completely wetted. Moreover, the equation presupposes a bulk liquid phase which is not exactly the case. Even so the results appear to be consistent.

We have also estimated the size of the critical nucleus for the freezing process starting at configurations not completely melted containing residual crystallites, by analysing the solid portion of the cluster remaining at the final stage of the melting process. The maximum energy where the residual crystallite constitutes an effective nucleus is taken from the crossing point of the melting and recrystallisation curves (black and blue curves in Fig. 1). The size of the crystallite is then estimated by interpolation of the liquid molar fractions. Table 6 contains the results for clusters of different sizes together with the ones for heterogeneous nucleation. Fig. 9 displays the inverse of the average number of particles by one edge of the cubic nucleus as a function of temperature. Note that the straight line approach 0 as $T \to T_m$ according to Eq. (6). Considering that the method used to compute the results referring to residual crystallites is a bit crude and that, in the two sets of results, the nuclei are differently wetted it seems that there is a fairly good regular behaviour.

4. Phase coexistence model

An exact and complete treatment of phase coexistence would require the partition function of the system [49,50]. This is a chal-

Table 6
Critical nuclei sizes $n_s = n_a^3$ as a function of the temperature (T/K) for KCl. a) from residual crystallites; b) from the seeding process. Between parenthesis is the number of ions used to collect the data.

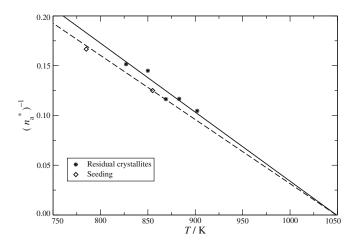| n_s	T		n
	(a)	(b)	
216		785	(5832)
290	875		(1000)
328	893		(1728)
512		855	(5832)
630	922		(2744)
634	905		(4096)
874	939		(5832)

Fig. 9. Inverse of the average number of particles by one edge of the cubic nucleus as a function of temperature for KCl clusters. Diamonds represent the values obtained from seeding, and the stars the values from residual crystallites.

lenging task, even for the simplest systems [51,52], but restrictive approximations are generally unavoidable [53].

The partition function approach, however, plays an important role in the study of very small systems that are not able to sustain phase coexistence [53,54]. These systems either dynamically oscillate between ordered and disordered conformations [53] (observed up to around 100 ions for alkali-halides [16]) or present sharp jumps between the ordered and disordered phases in the form of hysteresis cycles when heated and cooled (observed from near 100 up to around 1000 ions for alkali-halides [16]).

Larger systems presenting sustained phase coexistence (in the form of two regions, one ordered (solid) and the other disordered (liquid) separated by a permanent interface) require a different approach. That is the case for the alkali-halides clusters with sizes over 1000 ions presented in Section 3. Making geometric restrictions to the shapes of the component phases, it is possible to obtain a relation between the system variables [43]. However, even for the simplest geometries, the equations obtained by this method may become very intricate. A less restrictive model in what concerns to solid and, specially, to liquid shapes, proposed by us [19], is discussed in what follows.

Clusters behave differently from the corresponding bulk systems, mainly in phase change or phase coexistence regions. However, they asymptotically approach the bulk properties as the size increases. This is just the basis of the proposed model. It is assumed that a given cluster has a virtual bulk-like behaviour which is taken as the reference state. The model traces out the deviations (dependent on the number of particles, n) relatively to the reference state. All the derived equations should then yield the right bulk limit when $n \to \infty$.

The size of the cubic critical nucleus, n^*, (taking the power 3 of Eq. (6))

$$n^* = \left[\frac{4\upsilon^{\frac{2}{3}}\sigma T_m}{(T_m - T)\Delta h} \right]^3 \tag{9}$$

approaches infinity at the bulk melting temperature, T_m. According to the results presented in Section 3.2.3, it is assumed that Eq. (9) is a fairly good approximation even when the liquid phase is not infinite and the nucleus is not completely wetted. The size of the cubic critical nucleus can be recast in a more compact form:

$$n^* = k^3 \frac{T_m^{\ 3}}{(T_m - T)^3} \tag{10}$$

where

$$k^3 = \left[\frac{4\upsilon^{\frac{2}{3}}\sigma}{\Delta h} \right]^3 \tag{11}$$

In a bulk system, after the melting onset and solid–liquid equilibrium is attained, adding energy to the system converts a portion of solid to liquid, with the temperature and pressure remaining constant. The number of solid ions in the bulk system, n_s^∞, at a given energy E, is:

$$n_s^\infty = \frac{E_{l(T_m)} - E}{E_{l(T_m)} - E_{s(T_m)}} n \tag{12}$$

where $E_{s(T_m)}$ and $E_{l(T_m)}$ are, respectively, the total energies of the bulk solid and liquid at the melting temperature T_m, and n is the total number of particles in the system.

A finite system (cluster) prepared at any fixed total energy over the bulk solid–liquid line shall always have a size less than the critical nucleus (see Eq. (9) at T_m. At those fixed energies a number of solid ions, Δn_s, shall be transferred to the liquid until the cluster reaches a temperature $T < T_m$ at which the corresponding solid critical nucleus can sustain equilibrium with the liquid. If the conversion of solid ions into liquid was realised at constant temperature, it would require an external energy $[\Delta n_s/n]\Delta h$, to compensate for the increase of potential energy. For the clusters at constant total energy the increase of potential energy is entirely obtained at the cost of the internal kinetic energy. This results in a decrease of the cluster temperature, $\Delta T = T - T_m$,

$$\Delta T = \frac{\Delta n_s \Delta h}{n C_p} \tag{13}$$

where Δh is the enthalpy of melting and C_p is the heat capacity.

The number of solid ions in the cluster, at energy E, as a function of temperature is obtained from:

$$n_s = n_s^{bb} + \Delta n_s \tag{14}$$

where n_s^{bb}, given by the same form of Eq. (12), should be understood as the number of solid ions that the cluster would have if it followed the bulk behaviour. $E_{s(T_m)}$ and $E_{l(T_m)}$ are, now, the projected solid and liquid cluster energies at the bulk melting temperature, T_m, which depend, of course, on the cluster size. Substituting n_s^{bb} from 12 and Δn_s from 13:

$$n_s = \frac{E_{l(T_m)} - E}{\Delta h} n + \frac{(T - T_m)n C_p}{\Delta h} \tag{15}$$

In a first order approximation, we can take the bulk value for $\Delta h = E_{l(T_m)} - E_{s(T_m)}$ [18]. However, Δh is also a function of the number of particles. This aspect shall be taken into account in a second order approximation presented in subsection 4.1. Incidentally, it is noteworthy that Eq. (15) yields the right bulk limit when $n \to \infty$, where $(T - T_m) = 0$. Relatively to C_p, it seems plausible to take it, in a first approximation, as the average of the solid and liquid values at the start and end of melting, since that values do not differ much for alkali halide clusters [17] (see Tables 7 and 8). However, for

Table 7
Enthalpy of melting Δh (kJ mol^{-1}) and heat capacities C_p (JK^{-1} mol^{-1}) of solid and liquid NaI clusters at temperature $T_m = 933$K.

n	$C_p^{(s)}$	$C_p^{(l)}$	Δh
1000	75.19	69.58	17.53
1728	68.01	70.53	19.37
2744	68.27	68.96	19.52
4096			
∞			
Exp.	59.95	64.85	23.60

Table 8
Enthalpy of melting, Δh (kJ mol^{-1}), and heat capacities, C_p (JK^{-1} mol^{-1}) of NaCl solid and liquid clusters at temperature T_m = 1074 K.

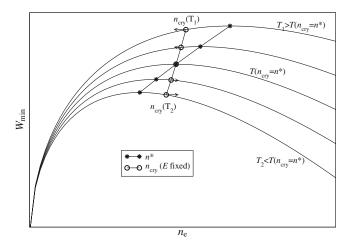| n	$C_p^{(s)}$	$C_p^{(l)}$	Δh
1000	69.03	70.57	23.80
1728	67.44	70.67	24.38
2744	66.90	70.70	24.97
4096	66.74	69.70	25.25
∞			27.75
Exp.	67.36	70.37	28.25

Fig. 10. Dynamics through which a cluster attains a solid–liquid equilibrium.

systems which have very distinct solid and liquid heat capacities a better approximation may be needed.

Accordingly to Eq. (9), the size of the critical nucleus depends on the temperature. A walk over embryos sizes, despite it remains driven in each moment by the work function slope for the respective size, carries the system over the work functions themselves. Fig. 10 captures, qualitatively, the essential dynamics through which a cluster can sustain a solid–liquid coexistence, at constant energy and external pressure. Suppose, for example, a solid crystallite of size $n_e(T_1)$ at temperature T_1. Once its size is less then $n^*(T_1)$, the cluster spontaneously melts and the crystallite shrinks. As the total energy is fixed, the temperature shall decrease until the crystallite size reaches the value $n^*(T)$, which also constitutes a critical nucleus, but now over a different work function surface. For sizes less than $n^*(T)$, for example at $T_2 < T$, the crystallite would spontaneously grow (with a temperature increase at constant total energy), since such size is greater than the critical nucleus of the corresponding work functions. As a consequence, phase equilibrium is attained when the crystallite size, given by Eq. (15), becomes equal to the size of the critical nucleus, given by Eq. (10), that is, when the temperature T is a root of:

$$\frac{E_{l(T_m)} - E}{\Delta h} n + \frac{(T - T_m)nC_p}{\Delta h} - k^3 \frac{T_m^3}{(T_m - T)^3} = 0 \tag{16}$$

From Eq. (16):

$$E = E_{l(T_m)} + (T - T_m)C_p - k^3 \frac{\Delta h T_m^3}{n(T_m - T)^3} \tag{17}$$

This is the key equation to predict (T,E) values for direct comparison with the results from simulations.

Fig. 11 represents the crystallite (n_s) and critical nucleus (n^*) sizes, at different energies, as a function of temperature, given by Eqs. (15) and (10), respectively. The lower temperature where
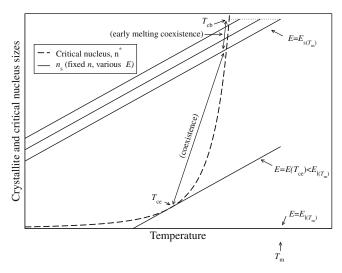

Fig. 11. Construction, built from Eqs. (15) and (10), to determine the limits of the phase coexistence for an arbitrary cluster.

coexistence still exists (coexistence end[2]) can be obtained noting that 15 and 10 are tangent at that point (see Fig. 11)

$$T_{ce} = T_m - \left(\frac{3k^3 T_m^3 \Delta h}{nC_p}\right)^{\frac{1}{4}} \tag{18}$$

and the correspondent energy is

$$E(T_{ce}) = E_{l(T_m)} + \frac{\Delta h}{n}\left[\frac{\Delta T nC_p}{\Delta h} + \frac{k^3 T_m^3}{(\Delta T)^3}\right] \tag{19}$$

where $\Delta T = T_{ce} - T_m$. The lowest energy where coexistence, predicted by Eq. (16), is possible (coexistence begin[3]) can be obtained noting that the temperature along the solid curve, near the melting point, is

$$T_s = T_m - \frac{E_{s(T_m)} - E}{C_p} \tag{20}$$

and equating it to temperature T in Eq. (10) with $n^* = n$:

$$E_{cb} = E_{s(T_m)} - kC_p T_m n^{-\frac{1}{3}} \tag{21}$$

Melting in the energy interval $]E_{cb}, E_{s(T_m)}[$ shall be, from now on, designated by "early melting", since the bulk-like conditions have been chosen as the reference ones for clusters. However, this does not mean an exceptional situation. Indeed, at the present approximation level, the model always predicts the cluster melting onset at lower temperatures and energies than the ones of the corresponding bulk systems.

The temperature correspondent to the energy E_{cb} is (see Fig. 11)

$$T_{cb} = T_m(1 - kn^{-\frac{1}{3}}) \tag{22}$$

The domain of T values for the resolution of the equation model in order to E is bounded by T_{cb} and T_{ce}.

4.1. Second order approximation to Δh

The dependence of Δh on the number of particles can be found considering:

---

[2] The notation T_{ce} and E_{ce} seems more clear than T_{inf} (for "inferior temperature") and E_{inf} that has been used in previous articles [19–22].

[3] The notation T_{cb} and E_{cb} seems also more clear than T_{if} (for "initiate fusion") and E_{if} that has been used in previous articles. [19–22].

$$E_{l(T_m)} = E_{l(T_m)}^{\infty} + \varsigma_l n^{-\frac{1}{3}} \qquad (23)$$

$$E_{s(T_m)} = E_{s(T_m)}^{\infty} + \varsigma_s n^{-\frac{1}{3}} \qquad (24)$$

hence

$$\Delta h = \Delta h^{\infty} + \Delta \varsigma n^{-\frac{1}{3}} \qquad (25)$$

The value of k is also dependent on n:

$$k = \frac{4 v^{\frac{2}{3}} \sigma}{\Delta h^{\infty} + \Delta \varsigma n^{-\frac{1}{3}}} \qquad (26)$$

The limit value $k^{\infty} = 4 v^{\frac{2}{3}} \sigma / \Delta h^{\infty}$ is obtained when $n \to \infty$. $\Delta \varsigma$ is the rate of change of the melting enthalpy with system size.

5. Examples of the model application

5.1. Minimum extent of supercooling

Additionally to the properties referred to above, as the energy and temperature at coexistence, the model predicts, for example, the minimum extent of supercooling that a droplet should attain, during the freezing process, before it can crystallise. It is defined by the ratio between the highest temperature where a cluster can start a liquid to solid transition and the melting temperature [19]. Fig. 12 shows the application to a series of KCl clusters, in comparison with the simulation results.

5.2. Liquid molar fractions

Properties of the system during the coexistence sates are also accessible. For example, the liquid molar fractions can be obtained from the ratio between the liquid portion and the total number of particles in the system:

$$\chi_{liq} = \frac{n - \left(\frac{kT_m}{T_m - T}\right)^3}{n} \qquad (27)$$

Fig. 13 shows the simulation results [17], obtained with the method based in the analysis of the velocity autocorrelation functions described elsewhere [16], compared with the model predictions for a KCl cluster with 4096 ions.
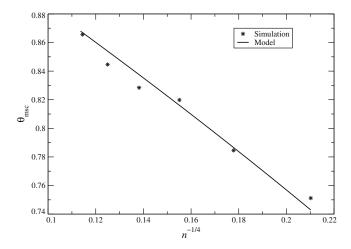
Fig. 12. Prediction of the minimum extent of supercooling as a function of system size for KCl clusters.
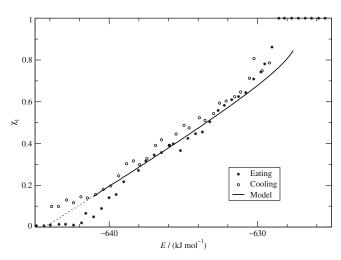
Fig. 13. Prediction of the liquid molar fraction as a function of energy for a 4096 ions KCl cluster. Simulation results from heating and cooling.
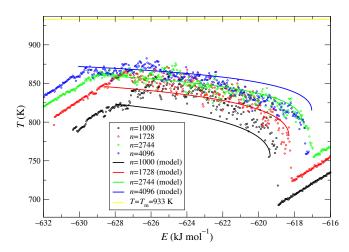
Fig. 14. Phase coexistence model prediction versus simulation results for a set of NaI cluster sizes.

5.3. Solid–liquid co-existence for NaI and NaCl clusters

Fig. 14 contains an example of the model application to predict the evolution of NaI clusters temperature as a function of the total energy and system size by using parameters $T_m = 933$ K, $k^{\infty} = 0.88$, $C_p = 69$ JK^{-1} mol^{-1}, $E_{l(T_m)}^{\infty} = -611.5$ kJ mol^{-1}, $\varsigma_l = 84.906$ kJ mol^{-1}, $\Delta h^{\infty} = 23.6$ kJ mol^{-1}, $\Delta \varsigma = -58$ kJ mol^{-1}. As expected, taking into consideration that the model assumes a bulk liquid phase (and the equations are considered only approximately valid for a finite liquid phase as already referred to), the predictions are more accurate for larger clusters. The more significant deviations, if any, tend to occur at the initial stages of the melting when the most part of the cluster is solid and the liquid part is just a small drop on a side or a thin layer on one or two faces. The model prediction divergence from the simulation results for the 4096 ions cluster above -622 kJ mol^{-1} is the exception to the general trend. This singular behaviour is suspected to be originated in a change from a partial wetting to a total immersion of the crystallite in the melt and requires further investigation. Therefore: (i) excluding the 4096 ions case, the melting end temperatures are correctly predicted; (ii) the melting start temperatures of the bigger clusters (2744 and 4096 ions) are in good agreement with simulations; (iii) the melting start temperatures of the smaller clusters (1000 and 1728 ions) are a bit underestimated; and (iv) early melting is observed accord-
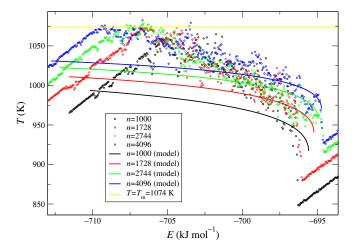
Fig. 15. Phase coexistence model prediction versus simulation results for a set of NaCl cluster sizes.
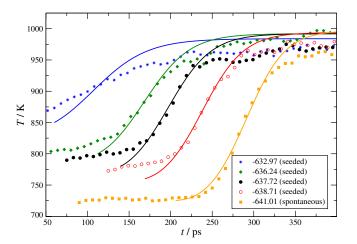

Fig. 16. Evolution in time of the KCl droplet+seed temperature predicted by Eq. (32). Symbols represent simulation results, lines the model predictions, and the inset the respective energies (kJ mol^{-1}).

ing to the model predictions similarly to what has been reported for LiCl clusters [20].

Fig. 15 contains the model prediction for the temperature evolution as a function of the energy in NaCl clusters by using the parameters $T_m = 1085$ K, $k^\infty = 0.72$, $C_p = 68$ JK^{-1} mol^{-1}, $E_{l(T_m)}^\infty = -690.98$ kJ mol^{-1}, $\varsigma_l = 106.16$ kJ mol^{-1}, $\Delta h^\infty = 27.74$ kJ mol^{-1}, $\Delta\varsigma = -39.647$ kJ mol^{-1}. In this case the simulations show that all clusters closely approach the bulk melting temperature, similarly to the case of KCl reported elsewhere [19]. However, the model predictions remarkably underestimate the melting temperature, suggesting early melting and contrary to the simulations. Nonetheless, the end parts of the coexistence curves are correctly predicted, remaining within the fluctuations observed for all clusters. Thus, NaCl clusters constitute a significantly less successful application of the model as far as early melting is concerned. Since the model failure is undoubtedly related to the approximations discussed above, in order to trace out perspectives that may aid in the overcoming of these limitations, a closer review of the model foundations is required.

5.4. Crystal growth dynamics

The phase coexistence model can also be used for the study of nonequilibrium processes as, for example, the crystal growth

dynamics, already referred to in Section 3.2, and here briefly discussed [21]. For a system with melting temperature T_m, the linear growth speed, u, of a nucleus of the stable phase at a given temperature T inside the infinite unstable phase (that is to say, the interface progression speed towards the stable phase) is given by Debenedetti's equation [11]

$$u = \frac{f k_B T}{3\pi a^2 \eta}\left\{1 - \exp\left[-\frac{\Delta h}{k_B T}\left(1 - \frac{T}{T_m}\right)\right]\right\} \tag{28}$$

where f is the fraction of the growing phase surface sites available for placing new particles, a is a number of the order of the molecular diameter and η is the viscosity.

For a solid–liquid phase transition in the case of a cubic solid nucleus, the change Δn_s in the number of particles in the solid nucleus n_s after a time Δt, for a system with density ρ, noting that $u\Delta t\rho^{1/3}$ is the average linear increase of the number of particles in the **u** direction, will be:

$$\Delta n_s = 6n_s^{\frac{2}{3}}u\rho^{\frac{1}{3}}\Delta t + O(\Delta t^2) \tag{29}$$

from which, removing higher order Δt terms:

$$\frac{\partial n_s}{\partial t} = 6n_s^{\frac{2}{3}}u\rho^{\frac{1}{3}} \tag{30}$$

Deriving 15 in order to t at a fixed energy, and considering the approximation that Δh and C_p are independent of temperature [19]:

$$\frac{\partial n_s}{\partial t} = \frac{nC_p}{\Delta h}\frac{\partial T}{\partial t} \tag{31}$$

Making use of Eqs. (15), (28), (31) and (30) and eliminating n_s, it results in

$$\frac{\partial T}{\partial t} = \alpha\left(\frac{E_{l(T_m)} - E + (T - T_m)C_p}{\Delta h}\right)^{\frac{2}{3}} \times T\left\{1 - \exp\left[-\frac{\Delta h}{k_B T}\left(1 - \frac{T}{T_{eq}}\right)\right]\right\} \tag{32}$$

with

$$\alpha = \frac{2\Delta h f k_B \rho^{\frac{1}{3}}}{\pi C_p a^2 \eta}n^{-\frac{1}{3}} \tag{33}$$

where T_{eq} represents the phase equilibrium temperature given by Eq. (16) [19].

Since Eq. (28) presupposes that nucleation is already realised, the model is not able to predict the starting time for the crystal growth process, but only its time evolution from there on. Moreover, once stationary conditions presupposed in Eq. (28) are not verified during stochastic formation of embryos, it should not be expected a perfect reproduction of experimental or simulation results at the early stages of the growth process. Nevertheless, Equation 32 is expected to give fairly good results for cluster sizes up to a few powers of ten, like the KCl ones for which we have simulation results available.

As we do not know the value of f, α has been obtained by a fit of Eq. (32) to the simulation data and then an estimation of f has been made. To this end, Eq. (32) has been solved numerically for a (5832–512) ions droplet seeded with a 512 ions crystallite (corresponding to $E = -638.71$ kJ mol^{-1} chosen from the droplet seeded cases studied in Ref. [17]) and α has been adjusted in order to minimise the deviations of the computed results from the simulated ones. The value of $\alpha = 1.88 \times 10^{-3}$ ps^{-1} has been obtained and used to predict the evolution for droplets at different energies, including a spontaneous nucleation case. The results are presented in Fig. 16 together with the correspondent ones simulated in the same conditions [17].

All curves present the expected sigmoid-like shape, starting with an approximate[4] cubic growth of the temperature (linearly related to n_s by Eq. (15) as the progressively larger (see Eq. (30) amount of the liquid converted to solid, per unit of time, proportionally converts potential energy into kinetic energy. This is followed by a strong slowdown, dictated by Eq. (28), near the equilibrium. There are, however, some relevant discrepancies between the simulation results and the model predictions which require a closer view. The differences observed at the initial stage of crystal growth are due to the perturbation that the seeding imposes on the temperature [17]. That is, the introduction of the seed directly drives the system to an intermediate stage of the crystal growth process. This is confirmed by the good agreement observed between the prediction, made using the same value of α, and the simulation results for the presented case of spontaneous nucleation. Such agreement is remarkable, considering the significant differences in the location of the nuclei at the early stages for the seeded and spontaneous cases.[5] However, as previously referred to, it is not expectable that the same level of agreement can be obtained at the initial stages for spontaneous nucleation at higher temperatures/energies (corresponding to higher sizes for the critical nuclei), since the stochastic contribution to the nuclei formation is not contained in the model.

6. Thermodynamic limit

Some cluster properties that we have computed from the simulations, and models, approach fairly well, mainly for larger clusters, the corresponding bulk properties determined by experiment or by simulations with a relatively small number of particles plus boundary conditions.

Given a cluster, not subjected to boundary conditions, how many particles should be used so that the simulated properties become indistinguishable from the bulk ones? Because of the huge computer time required, the way to answer such a question is not, of course, to perform direct simulations of successively larger clusters. Yet, we believe that is a valuable issue, either to clarify the operational meaning of "thermodynamic limit" or to estimate eventual errors involved in simulations to predict bulk properties of complex systems, by using small clusters as it is common, for example, in biochemical and electrochemical simulations.

Nonetheless, for some properties we can predict, in an indirect way, the clusters sizes in order to answer the question, based on linear or other convergence trends presented by the properties of large enough clusters, and on the relative deviation:

$$R(n) = \left| \frac{X_{ref} - X(n)}{X_{ref}} \right|, \tag{34}$$

where $X(n)$ is the value of a property for a n sized cluster and X_{ref} is the corresponding bulk value. Imposing a relative deviation we can compute

$$X(n) = (1 - R(n))X_{ref} \tag{35}$$

and in most cases the inverse function

$$n(X) = X^{-1}(n). \tag{36}$$

that allows to predict the cluster size under the imposed deviation.

Total energy values for solid clusters with sizes ranging from 64 to 8000 ions, presented in Table 9, show, for sizes above 512 ions, a

---

[4] Assuming that u is constant (a reasonable assumption for a small variation of T far from T_{eq}), the solution of Eq. (30) is $n_s = (2u\rho^{1/3}t + l)^3$, with $l = 0$ for spontaneous nucleation and l^3 equal to seed size for seeded cases.

[5] It should be noted that the spontaneous case was not followed strictly at fixed energy (see Fig. 1) but, instead, at a considerably slow decreasing rate of it. Although not very relevant, due to the small energy variation involved during most of the growth, correcting this aspect will even increase the agreement.

Table 9
Total energy, E(kJ mol^{-1}), at zero temperature and pressure, for solid clusters of KCl with sizes 64, 216, 512, 1000, 1728, 2744, 4096, 5832, 8000 and the bulk.

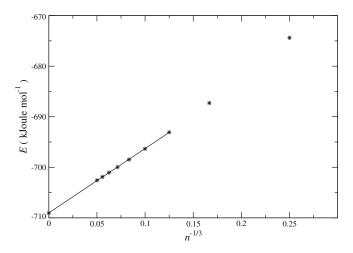| n	E	n	E
64	−674.392	2744	−699.968
216	−687.292	4096	−701.062
512	−693.068	5832	−701.910
1000	−696.354	8000	−702.574
1728	−698.480	Bulk	−709.052

Fig. 17. Total energy, E (kJ mol^{-1}), at zero temperature and pressure, for solid KCl clusters with sizes 64, 216, 512, 1000, 1728, 2744, 4096, 5832, 8000 and the bulk, represented as a function of $n^{-1/3}$.

well defined linear convergence to the bulk value, when represented as a function of $n^{-1/3}$ (see Fig. 17). Using Eqs. (35) and (36) the predicted system size that ensures less than 1% deviation in this property is $\simeq 10^4$.

If the same tolerance is used for free energies, reported elsewhere [22], the size predicted is also $\simeq 10^4$.

For the melting points in Table 1 there is no need for a convergence law to determine the cluster sizes within 1% deviation. In fact, for clusters with 1728 ions and above the computed values are systematically in this interval.

Heat capacities at 940 K, see Table 10, also show a linear convergence. Despite of the considerable uncertainty on the computed values, we can estimate from the fitted curve a cluster size of $\simeq 10^5$ within 1% deviation.

The number of particles on an edge of the critical nucleus, Eq. (7), can also be used to predict the minimum cluster size needed to have the possibility of spontaneous nucleation at temperature T. From

$$\frac{(T_m - T)}{T_m} \leqslant 0.01 \tag{37}$$

the number of particles on an edge of a KCl nucleus is 1.48/0.01 = 84, and a reasonable estimation of the cluster is $5 \times 148^3 \simeq 10^8$. This estimation assumes the maintenance of the proportion between critical nucleus and cluster sizes [17]. A more rigorous determination has been made from the model prediction for the minimum hysteresis extent, $\triangle T_{hist}$, that is, the minimum interval of temperatures where hysteresis is observed[19]:

$$\frac{\triangle T_{hist}}{T_m} = \left(3^{\frac{1}{4}} + 3^{-\frac{3}{4}}\right) \triangle h^{\frac{1}{4}} T_m^{-\frac{1}{4}} k^{\frac{3}{4}} (C_p n)^{-\frac{1}{4}} \leqslant 0.01 \tag{38}$$

from which, consistently, results

$$n \geqslant \left(3^{\frac{1}{4}} + 3^{-\frac{3}{4}}\right)^4 \triangle h T_m^{-1} k^3 C_p^{-1} 10^8 \simeq 10^8 \tag{39}$$

Table 10
Heat capacities C_p(JK^{-1} mol^{-1}) and total energies (kJ mol^{-1}) at temperatures 940 K and 1045 K, near the melting point, for the KCl cluster with sizes 512, 1000, 1728, 2744, 4096 and 5832.

n	940 K		1045 K	
	C_p	E_{tot}	C_p	E_{tot}
512	67.9	−640.17	–	–
1000	68.2	−643.70	–	–
1728	66.5	−645.95	–	–
2744	66.4	−647.46	–	–
4096	65.6	−648.56	71.9	−641.51
5832	63.6	−648.98	66.2	−642.17
From [42][a]	–	–	64.9	–
Exp. [42]	–	–	66.9	–
Exp. [39]	64.4	–	69.3	–

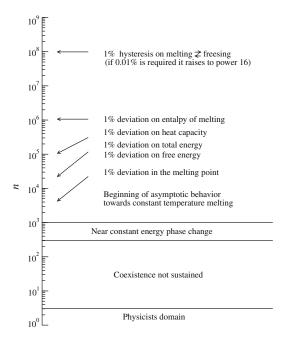[a] Obtained by interpolation of data in reference.

Fig. 18. Some examples of the thermodynamic limit border spreading depending on the system properties considered.

The results above are summarised in Fig. 18. It also marks some behaviour classes shown by the smaller clusters in terms of phase changing. The wide range of orders of magnitude covered is significant but becomes more impressive if nowadays experimental tolerances are used. In fact, the thermodynamic limit for experimental accuracy under 0.01%, a value accessible in the last two decades [55], requires a system size of 10^{12} for the enthalpy of melting and more than 10^{16} if hysteresis is considered.

7. Development perspectives

In the presented model, the slope of the work function dependence on the embryo size, $\mu = \Delta W / \Delta n_e$, that indicates the height of the free energy barrier, is evaluated supposing a bulk liquid phase, which constitutes a first approximation since clusters are finite systems. Therefore, additional constraints that can determine the states of the clusters should be considered regarding an extension of the model.

A partially melted finite system can be seen, depending on the proportions of the solid and liquid portions, either as a crystallite embryo in the presence of an unstable liquid, or as a droplet embryo in the presence of an unstable solid. As such, choosing the solid portion as parameter, we can define the family of functions $W_{liq}(n - n_s, T, p)$ that may present considerable free energy barriers to droplets formation, for $T < T_m$, like the ones presented by the family $W_{sol}(n_s, T, p)$ to crystallites formation for $T > T_m$. The respective slopes are μ_{liq} and μ_{sol}.

In this context, the following qualitative outline can be done, based on the behaviours observed in some of our simulations and the present model predictions:

1. $\mu_{liq} < \mu_{sol}$ and a droplet is easily formed even at temperatures significantly lower than T_m. Early melting is present and the phase coexistence extends from E_{if} to E_{inf} accordingly to the model (observed in LiCl and NaI clusters).

2. $\mu_{liq} > \mu_{sol}$ up to the neighbourhood of the bulk melting temperature, T_m, even for very small droplets. Nearly T_m the droplet formation barrier is overpassed and from there on the phase coexistence is in accordance with the model (observed in KCl clusters).

3. $\mu_{liq} > \mu_{sol}$ even at the neighbourhood of the bulk melting temperature, T_m. The system slightly overcomes T_m and starts melting in a overheated state until the droplet contribution becomes less significant and allows the proper crystallite contribution being attained by a fluctuation. Then, this is followed by a relatively sharp transition to the model predictions (observed in NaBr and NaCl clusters).

The outlined situations are not exhaustive. Moreover, the enumerated behaviours can be observed in the same cluster family when different sizes are considered. For example, the results for NaI clusters, in Fig. 14, show that for sizes 1000 and 1728 ions, despite they never come close to the bulk melting temperature, do not present a perfect early-melting, though the sizes 2744 and 4096 do. This means that the balance between the weights of the contributions from the crystallite and the droplet changes with size. Thus, a model extension clearly needs to include, at least, the quantitative contribution of the droplet work of formation, the surfaces of the systems, and the determination of the equilibrium states accessible taking into account, for each energy value, the complete system geometry in the spirit of the work by Cleveland et al. [43]. However, this is not a straightforward improvement due to the multiplicity of geometries that might be involved and it is still an open challenge.

Other improvements are being considered. For example, the need to deal with the vapour pressure of more volatile substances claims for an extension of the model. Despite alkali halide aggregates can be observed in the absence of applied external pressure for considerable lifetimes, significant values are expected for the internal pressure in small clusters because of the large fraction of surface particles and small surface curvature radius. The derivation of the internal pressure from the model, and its comparison with simulation results, is presently being assessed.

In the presented form, the model for crystal growth dynamics is only a first order approximation in several aspects. The more important of them is the assumption that heat flow along the cluster is instantaneous, and consequently that thermalization is always met. This is certainly not the situation for relatively large clusters. In these cases, a local differential equation, incorporating the heat flow process, should be used instead of a global one like Eq. (32). It is also important to mention that Eq. (28) is has not been used strictly in the conditions of its original derivation. Moreover, the use of a local equation to have an exact description of the problem implies the consideration of the system (crystallite + droplet) geometry, which is one of the other relevant aspects not yet considered. A more exact accounting of the solid and liquid contributions to C_p may also be important for higher order approximations.

Despite all these limitations, the model seems to capture fairly well the main trends of the crystal growth process inside an overcooled cluster. However, some discrepancies between the models predictions and the simulation results, involving fine structure effects (for example, the wavy behaviour of the simulations at the final stages, seen in Fig. 16), confirm that a model extension is needed. Indeed, only a local description of the system [56], complemented by adequate initial and boundary conditions, might improve the prediction of the system evolution. This is a considerable challenge due to the complexity of the phase regions geometries, and it is one of the perspectives to future work. As well as the extension of this study to other alkali halides, with a comparison between the respective values of f, and with experimental values if available.

Along the work development, comparison with experimental and simulation results obtained by other methods and authors has been done whenever possible. For example, during the free energy analysis of the lattices for LiCl clusters [20], molecular dynamics results from Croteau and Patey [57] and *ab initio* results from Aguado and collaborators [30] have been considered. In general a good agreement is observed. Yet, due to the limited results available in the literature for the same cluster sizes as ours, a direct comparison has been barely possible. We hope that the production of *ab initio* data for larger clusters series, presently under progress in our group, will overcome those limitations.

Acknowledgements

References

[1] J.J. Moura-Ramos, N.T. Correia, The Deborah number, relaxation phenomena and thermally stimulated currents, Phys. Chem. Chem. Phys. 3 (24) (2001) 5575–5578.
[2] J.B. Kaelberer, R.D. Etters, Phase transitions in small clusters of atoms, J. Chem. Phys. 66 (7) (1977) 3233–3239.
[3] N. Quirke, Ping Sheng, The melting behaviour of small clusters of atoms, Chem. Phys. Lett. 110 (1) (1984) 63–66.
[4] S.M. Thompson, K.E. Gubbins, J.P.R.B. Walton, R.A.R. Chantry, J.S. Rowlinson, A molecular dynamics study of liquid drops, J. Chem. Phys. 81 (1) (1984) 530–542.
[5] Y. Sakamoto, Thermodynamic and static properties of alkali halide microclusters, J. Phys. Soc. Jpn 59 (11) (1990) 3925–3930.
[6] J.P. Rose, R.S. Berry, Towards elucidating the interplay of structure and dynamics in clusters: small KCl clusters as models, J. Chem. Phys. 96 (1) (1992) 517–538.
[7] J.P. Rose, R.S. Berry, Freezing, melting, nonwetting, and coexistence in (KCl)$_{32}$, J. Chem. Phys. 98 (4) (1993) 3246–3261.
[8] J.P. Rose, R.S. Berry, (KCl)$_{32}$ and the possibilities for glassy clusters, J. Chem. Phys. 98 (4) (1993) 3262–3274.
[9] F.M.S.S. Fernandes, L.A.T.P. Neves, Phase transitions in ionic clusters, Am. Inst. Phys. Conf. Proc. 330 (1995) 313.
[10] H. Deng, J. Huang, Molecular dynamics studies of the kinetics of phase changes in clusters: Crystal nucleation of (rbcl)108 clusters at 600, 550, and 500 K, J. Solid State Chem. 159 (2001) 10–18.
[11] P.G. Debenedetti, Metastable Liquids, Concepts and Principles, Princeton University Press, New Jersey, 1996.
[12] S. Sugano, H. Koizumi, Microcluster Physics, Springer, 1998.
[13] J.K. Lee, J.A. Barker, F.F. Abraham, Theory and Monte Carlo simulation of physical clusters in the imperfect vapor, J. Chem. Phys. 58 (8) (1973) 3166.
[14] F. Calvo, P. Labastie, Melting and phase space transitions in small ionic clusters, J. Phys. Chem. B 102 (11) (1998) 2051–2059.
[15] J.E. Adams, R.M. Stratt, New insight into experimental probes of cluster melting, J. Chem. Phys. 93 (2) (1990) 1358–1368.
[16] P.C.R. Rodrigues, F.M.S.S. Fernandes, Molecular dynamics of phase transitions in clusters of alkali halides, Int. J. Quant. Chem. 84 (2) (2001) 169–180.
[17] P.C.R. Rodrigues, F.M.S.S. Fernandes, Melting, freezing and nucleation in nanoclusters of potassium chloride. I. Molecular dynamics simulation, Eur. Phys. J. D 40 (1) (2006) 115–123.
[18] P.C.R. Rodrigues, Transições de Fase em Sistemas Iónicos, Modelos Teóricos e Simulação Computacional, PhD thesis, Faculdade de Ciências, Universidade de Lisboa, 2006.
[19] P.C.R. Rodrigues, F.M.S.S. Fernandes, Melting, freezing and nucleation in nanoclusters of potassium chloride. II. Modelling the solid–liquid coexistence, Eur. Phys. J. D 41 (1) (2007) 113–119.
[20] P.C.R. Rodrigues, F.M.S.S. Fernandes, Cubic and hexagonal symmetries in LiCl nanoclusters, Eur. Phys. J. D 44 (2007) 109–116.
[21] P.C.R. Rodrigues, F.M.S.S. Fernandes, Melting, freezing and nucleation in nanoclusters of potassium chloride. III. Modelling crystal growth dynamics, Eur. Phys. J. D 47 (2008) 373–377.
[22] P.C.R. Rodrigues, F.M.S.S. Fernandes, Free energies of ionic nanoclusters, solid and coexistent solid–liquid states, Eur. Phys. J. D 49 (3) (2008) 353–359.
[23] A.V. Egorov, E.N. Brodskaya, A. Laaksonen, Solid–liquid phase transition in small water clusters: a molecular dynamics simulation study, Mol. Phys. 1000 (7) (2002) 941–951.
[24] M. Schmidt, H. Haberland, Phase transitions in clusters, C.R. Physique 3 (3) (2002) 327–340.
[25] A. Proykova, S. Pisov, R.S. Berry, Dynamical coexistence of phases in molecular clusters, J. Chem. Phys. 115 (18) (2001) 8538–8591.
[26] A. Proykova, D. Nikolova, R.S. Berry, Symmetry in order–disorder changes of molecular clusters, Phys. Rev. B 65 (8) (2002) Art. No. 085411.
[27] A. Vichare, D.G. Kanhere, S.A. Blundell, Model dependence of the thermodynamic properties of Na-8 and Na-20 clusters studied with ab initio electronic structure methods, Phys. Rev. B 64 (4) (2001).
[28] A. Aguado, J.M. López, J.A. Alonso, M.J. Stott, Melting in large sodium clusters: an orbital–free molecular dynamics study, J. Phys. Chem. B 105 (12) (2001) 2386–2392.
[29] A. Aguado, L.E. González, J.M. López, Thermal properties of impurity-doped clusters: orbital-free molecular dynamics simulations of the melting-like transition in li$_1$na$_{54}$ and cs$_1$na$_{54}$, J. Phys. Chem. B 108 (31) (2004)11722–11731.
[30] A. Aguado, A. Ayuela, J.M. Lopez, J.A. Alonso, Structure and bonding in small neutral alkali halide clusters, Phys. Rev. B 56 (23) (1997) 15353–15360.
[31] A. Vegiri, S.V. Schevkunov, A molecular dynamics study of structural transitions in small water clusters in the presence of an external electric field, J. Chem. Phys. 115 (9) (2001) 4175–4185.
[32] X. Campi, H. Krivine, N. Sator, Clustering and thermodynamics in small systems, Nucl. Phys. A681 (2001) 458c–465c.
[33] R.O. Watts, I.J. McGee, Liquid State Chemical Physics, John Wiley and Sons, 1976, pp. 307–312.
[34] J. Michielsen, P. Woerlee, F.V.D. Graaf, J.A.A. Ketelaar, Pair potential for alkali-metal halides with rock salt crystal-structure – molecular-dynamics calculations on NaCl and LiI, J. Chem. Soc., Faraday Trans. II 71 (1975) 1730–1741.
[35] P.C.R. Rodrigues, F.M.S.S. Fernandes, Phase diagrams of alkali halides using two interaction models: a molecular dynamics and free energy study, J. Chem. Phys. 126 (02) (2007) 024503.
[36] M.P. Allen, D.J. Tildesley, Computer Simulation of Liquids, Claredon Press, Oxford, UK, 1987.
[37] E.R. Buckle, A.R. Ubbelohde, Studing on the freezing of pure liquids. I. Critical supercooling in molten alkali halides, Proc. Roy. Soc. A 259 (1960) 325.
[38] P.J. Linstrom, W.G. Mallar, (Eds.), NIST Chemistry WebBook, NIST Standard Reference Database Number 69, National Institute of Standards and Technology, Gaithersburg MD, 20899, March 2003.
[39] M.W. Chase, Jr., Untitled. J. Phys. Chem. Ref. Data, Monograph 9, 27 (6) (1998).
[40] S. Rice, W. Klemperer, Thermodynamic properties of the gaseous alkali halides, J. Chem. Phys. 27 (3) (1957) 643–645.
[41] A.S. Dworkin, M.A. Bredig, The heat of fusion of the alkali metal halides, J. Phys. Chem. 64 (2) (1960) 269–272.
[42] L.V. Woodcock, K. Singer, Thermodynamic and structural properties of liquid ionic salts obtained by Monte Carlo computation. Part I. Potassium chloride, Trans. Faraday Soc. 67 (577) (1971) 12–30.
[43] C.L. Cleveland, U. Landman, W.D. Luedtke, Phase coexistence in clusters, J. Phys. Chem. 98 (25) (1994) 6272–6279.
[44] L.V. Woodcock, C.A. Angell, P. Cheeseman, Molecular dynamics studies of the vitreous state: simple ionic systems and silica, J. Chem. Phys. 65 (4) (1976) 1565–1577.
[45] P.C.R. Rodrigues, F.M.S.S. Fernandes, Animation of the melting of a kcl cluster, 2009. http://elixir.dqb.fc.ul.pt/clusters/melt.avi.2009.
[46] P.C.R. Rodrigues, F.M.S.S. Fernandes, Animation of the successful seeding of a kcl droplet, 2009. http://elixir.dqb.fc.ul.pt/clusters/seeded.avi.
[47] P.C.R. Rodrigues, F.M.S.S. Fernandes, Animation of the unsuccessful seeding of a kcl droplet, 2009. http://elixir.dqb.fc.ul.pt/clusters/failedseed.avi.
[48] I.V. Markov, Crystal Growth for Beginners, third ed., World Scientific Publishing Co. Pte. Ltd., Singapore, 1998.
[49] D. Ruelle, Statistical Mechanics, Rigorous Results, Benjamin, New York, 1969.
[50] K. Huang, Statistical Mechanics, John Wiley and Sons, New York, 1987.
[51] L. Onsager, Crystal statistics. I. A two-dimensional model with an order–disorder transition, Phys. Rev. 65 (3 and 4) (1944) 117–149.
[52] A.E. Ferdinand, M.E. Fisher, Bounded and inhomogeneous Ising models. I. Specific-heat anomaly of a finite lattice, Phys. Rev. 185 (2) (1969) 832–846.
[53] J.E. Adams, R.M. Stratt, Instantaneous normal mode analysis as a probe of cluster dynamics, J. Chem. Phys. 93 (2) (1990) 1332–1346.
[54] R.S. Berry, B.M. Smirnov, Two-state approximation for aggregate states of clusters, J. Chem. Phys. 114 (15) (2001) 6816.
[55] Y. Sato, T. Ejima, M. Fukasawa, K. Abe, Surface tensions of molten alkali-metal halides, J. Phys. Chem. 94 (5) (1990) 1991–1996.
[56] Alan J. Bray, Coarsening dynamics of nonequilibrium phase transitions, in: M.E. Cates, M.R. Evans (Eds.), Soft and Fragile Matter, Institute of Physics Publishing, Bristol, 2000. pp. 205–234.
[57] T. Croteau, G.N. Patey, Structures and rearrangements of LiCl clusters, J. Chem. Phys. 124 (2006) 244506.